

**University of Dundee**

## **Iron coral**

Li, Qianwei; Liu, Daoqing; Wang, Tongzhe; Chen, Chunmao; Gadd, Geoffrey Michael

*Published in:*  
Chemical Engineering Journal

*DOI:*  
[10.1016/j.cej.2020.126263](https://doi.org/10.1016/j.cej.2020.126263)

*Publication date:*  
2020

*Licence:*  
CC BY-NC-ND

*Document Version*  
Peer reviewed version

[Link to publication in Discovery Research Portal](#)

### *Citation for published version (APA):*

Li, Q., Liu, D., Wang, T., Chen, C., & Gadd, G. M. (2020). Iron coral: Novel fungal biomineralization of nanoscale zerovalent iron composites for treatment of chlorinated pollutants. *Chemical Engineering Journal*, 402, Article 126263. <https://doi.org/10.1016/j.cej.2020.126263>

### **General rights**

Copyright and moral rights for the publications made accessible in Discovery Research Portal are retained by the authors and/or other copyright owners and it is a condition of accessing publications that users recognise and abide by the legal requirements associated with these rights.

### **Take down policy**

If you believe that this document breaches copyright please contact us providing details, and we will remove access to the work immediately and investigate your claim.

# Iron coral: novel fungal biomineralization of nanoscale zerovalent iron composites for treatment of chlorinated pollutants

*Qianwei Li<sup>1,†</sup>, Daoqing Liu<sup>2,3,†</sup>, Tongzhe Wang<sup>1</sup>, Chunmao Chen<sup>1,\*</sup>, and Geoffrey*

*Michael Gadd<sup>1,4</sup>*

<sup>1</sup>State Key Laboratory of Heavy Oil Processing, State Key Laboratory of Petroleum Pollution Control, China University of Petroleum-Beijing, Beijing 102249, China

<sup>2</sup>Department of Environmental Engineering, Peking University, Beijing 100871, China

<sup>3</sup>The Key Laboratory of Water and Sediment Sciences, Ministry of Education, Beijing 100871, China

<sup>4</sup>Geomicrobiology Group, School of Life Sciences, University of Dundee, Dundee DD1 5EH, Scotland, UK

\*Corresponding author: Chunmao Chen, [chunmaochan@163.com](mailto:chunmaochan@163.com)

<sup>†</sup>both authors contributed equally to this work.

**Key words:** fungal biomineralization; nZVI, chlorinated pollution; geochemical simulation

## Abstract

In this research, a facile fungal biomineralization method was developed for the synthesis of nanoscale zerovalent iron (nZVI) with a unique N-doped branching structure, which showed excellent stability and mediated high degradation of carbon tetrachloride (CCl<sub>4</sub>) in aqueous solution. The ureolytic fungus *Neurospora crassa* was cultured in medium containing Fe<sup>2+</sup> and urea which resulted in iron carbonate biomineral precipitation. Following carbonization at 900°C, the fungal-carbonate composite became highly porous and granular nanoparticles (~50 nm diameter) were distributed evenly around the carbonized hyphae in a coralline manner. This ‘iron coral’ composite was identified as a mixture of zerovalent iron (Fe<sup>0</sup>), carbon iron (Fe<sub>1.91</sub>C<sub>0.09</sub>) and iron oxide (Fe<sub>3</sub>O<sub>4</sub>). The porous branching hyphal framework improved the capture efficiency of CCl<sub>4</sub>, and the N-doped sites may accelerate the electron transfer between CCl<sub>4</sub> and nZVI. Geochemical simulation was applied to verify the formation of the biominerals, and chemical analyses confirmed its significant degradation ability for CCl<sub>4</sub>. These findings have therefore demonstrated that ureolytic fungi can provide a promising environmental-friendly system for the novel preparation of nZVI through biomineralization with the resulting ‘iron coral’ capable of significant removal of a chlorinated compound and therefore indicating new bioremediation applications.

## 1 **1. Introduction**

2 Chlorinated pollutants are the most common organic pollutants in groundwater which can  
3 cause serious problems for ecosystems and human health due to their volatility, carcinogenic  
4 effects and bioaccumulation potential [1]. Over the last three decades, zerovalent iron (ZVI)  
5 has been extensively applied for the remediation or removal of chlorinated substances,  
6 including hydrocarbons, from contaminated aqueous solution [2-5]. ZVI technology research  
7 has been mainly focused in three contexts: development of various synthesis methods to  
8 overcome limitations of ZVI during remediation applications; exploring the possibility of ZVI  
9 for the removal of novel contaminants arising from modern industrial and agricultural  
10 technologies; and practical applications of ZVI in contaminated sites [1, 5, 6]. Although ZVI  
11 can exhibit excellent performance in contaminant removal, nanoscale ZVI (nZVI) particles  
12 offer a much higher potential due to their large specific surface area, high reactivity and  
13 adequate mobility [7, 8]. However, nanoscale particles tend to aggregate due to weak van der  
14 Waals forces, high surface energy and intrinsic magnetic interactions which results in a  
15 decrease in the number of active sites and reduced mobility thus limiting reaction efficiency  
16 and practical applications [4].

17 To improve dispersion and avoid nanoparticle aggregation, research has been carried out on  
18 the synthesis of novel nZVI-based materials, including surface modified nZVI (e.g., by  
19 chitosan or carboxyl methylated cellulose coatings and amino-functionalized nZVI) [8-10] and  
20 solid materials supporting nZVI (e.g., activated carbon, graphene and organic resins) [2, 11,  
21 12]. A novel stabilized nZVI-Ni catalyst was developed using polyvinylpyrrolidone (PVP) and  
22 this exhibited better mobility than bare nZVI-Ni [13]. The stabilized nZVI-Ni could degrade  
23 trichloroethylene (TCE) completely in 1 h with superior dechlorination kinetics. Carbon-based  
24 materials, e.g. activated carbon, graphene, and carbon nanotubes, have been evaluated as  
25 important supporting materials for nZVI due to their high surface area, gap structure and other

26 unique properties [14]. Graphene-supported nZVI (G-nZVI) was prepared for the removal of  
27 trichlorinitromethane (TGNM) from drinking water and 99% of TGNM was adsorbed and  
28 degraded using a 60 mg l<sup>-1</sup> G-nZVI dosage within 120 min [15]. Although stabilized and solid  
29 supported nZVI can exhibit high dispersibility and reactivity, several stabilizing agents have  
30 been reported to compete for nZVI active sites with contaminants while a stable distribution of  
31 nZVI on solid supports is hard to achieve [4, 16].

32 In the natural environment, fungi can interact with metal and minerals through various  
33 biomineralization, biosorption and biotransformation processes, which can be key components  
34 of biogeochemical cycles [17-20]. Biomineralization is the process of mineral formation by  
35 organisms and the final products commonly contain organic and inorganic components [17,  
36 19]. One mechanism for the biomineralization of metal carbonates is related to urea  
37 degradation. In a growth medium or habitat containing urea, ureolytic microorganisms degrade  
38 urea and release ammonium (NH<sub>4</sub><sup>+</sup>) and carbonate (CO<sub>3</sub><sup>2-</sup>) ions, the latter reacting with free  
39 metal ions resulting in the precipitation of metal carbonates [17]. The surfaces of the branching  
40 mycelial network of filamentous fungi provide nucleation sites for mineral precipitation.  
41 Moreover, the secretion of metabolites (e.g. extracellular proteins, polysaccharides, amino  
42 acids, and organic acids) also play important roles in the formation of nano- and microscale  
43 minerals [21]. Previous research has demonstrated that the urease-positive fungi *Neurospora*  
44 *crassa*, *Pestalotiopsis* sp. and *Myrothecium gramineum* were able to precipitate toxic metal  
45 ions (e.g. Co<sup>2+</sup>, Zn<sup>2+</sup>, Cd<sup>2+</sup>, Cu<sup>2+</sup> and Ni<sup>2+</sup>) as carbonates in a urea-modified medium [19, 22,  
46 23]. It was shown that extracellular protein was responsible for governing mineral size and  
47 morphology and further studies proved that in the biomineralization process, the conformation  
48 of extracellular proteins preferentially formed β-structures rather than α-helices [23]. Excreted  
49 amino acids, such as L-glutamic acid, were found to stabilize copper-containing minerals in  
50 the early stages of crystal growth and prevented crystal aggregation which resulted in the

51 bioprecipitation of nanoparticles [21]. Moreover, fungal biomass has been developed as a  
52 carbon precursor for various applications including electrochemical materials and  
53 electrocatalysis, through biomineralization and subsequent carbonization [22, 24]. In the  
54 process of biomineralization, the cross-linked branching hyphal structure can provide  
55 mechanical support and **significant properties for the enhanced dispersion of reactants**. The aim  
56 of this research was to examine the fungal biomineralization of **nZVI** by ureolytic fungi to  
57 provide understanding of the mechanisms involved and to identify possible applications for the  
58 degradation or bioremediation of chlorinated pollutants.

## 59 2. Materials and methods

### 60 2.1 Geochemical simulation of iron carbonate precipitation using Geochemist's 61 Workbench (GWB)

62 Previous studies have demonstrated that ureolytic fungi can precipitate metal carbonates (e.g.  
63  $\text{CaCO}_3$ ,  $\text{SrCO}_3$  and  $\text{CoCO}_3$ ) in a carbonate-laden system produced by ureolysis [17-19, 21]. To  
64 understand the solubility of  $\text{Fe}^{2+}$  in the fungal biomineralization system, GWB 11.0.6 (Aqueous  
65 Solutions LLC, Urbana-Champaign, USA) was applied for the geochemical simulation of iron  
66 carbonate bioprecipitation, and this software can be used for the calculation of stability  
67 diagrams and determination of the chemical equilibrium states in aqueous solutions. Further  
68 details and application of the GWB software to examine carbonate bioprecipitation can be  
69 found in Li et al. [23]. In these experiments, the concentration of  $\text{CO}_3^{2-}$  was set as 330 mM  
70 (330 mM urea is completely degraded by ureolytic fungi incubated in AP1 media producing  
71 equimolar carbonate [23]) and the other set components were the same as in the AP1 medium  
72 (6.1 mM  $\text{Cl}^-$ , 0.83 mM  $\text{SO}_4^{2-}$ , 0.66 M  $\text{NH}_4^+$ , 4 mM  $\text{K}^+$ , 0.8 mM  $\text{Mg}^{2+}$ , 1.7 mM  $\text{Na}^+$ , 0.2 mM  
73  $\text{Ca}^{2+}$ , 0.02 mM  $\text{Mn}^{2+}$ , 0.01 Mm  $\text{Zn}^{2+}$  and 9  $\mu\text{M}$   $\text{Fe}^{3+}$  at 25°C). According to previous  
74 experimentation, the pH of fungal supernatants was between pH 7.0 and 8.0 after incubation in  
75 urea-containing media and therefore minerals precipitated in this pH range will be investigated  
76 in the simulation system.

77

### 78 2.2 Biomineralization of Fe-containing minerals by *Neurospora crassa*

79 The experimental fungus used was *Neurospora crassa* (WT ACCC #32256, Agricultural  
80 Culture Collection of China (ACCC), Beijing, China). It was grown in malt extract (ME) liquid  
81 medium in a shaking incubator in the dark (125 rpm, 25°C). After 3 d incubation, fungal  
82 biomass was filtered using a sterilized sieve (80 mesh, i.e. 80 squares per linear inch, equivalent  
83 to squares of dimension 180 x 180  $\mu\text{m}$ ), resuspended in sterilized Milli-Q water and filtered

84 again. Fungal biomass was transferred to a modified liquid medium (AP1) for mineral  
85 precipitation. AP1 medium contained 111 mM glucose, 0.33 M urea, 4 mM K<sub>2</sub>HPO<sub>4</sub>, 0.8 mM  
86 MgSO<sub>4</sub>, 0.2 mM CaCl<sub>2</sub>, 2 mM NaCl and trace metals 1.4 × 10<sup>-2</sup> mM ZnSO<sub>4</sub>, 1.8 × 10<sup>-2</sup> mM  
87 MnSO<sub>4</sub>, and 1.6 × 10<sup>-3</sup> mM CuSO<sub>4</sub>. To obtain an appropriate amount of biominerals (iron  
88 carbonate) and ensure good growth of *N. crassa*, 10 and 20 mM Fe<sup>2+</sup> were the final  
89 concentrations chosen for mineral precipitation in liquid medium. The FeSO<sub>4</sub> stock solutions  
90 (0.4 M) were filtered using 0.2 μm pore size membrane filters (Sartorius Stedim Biotech,  
91 Göttingen, Germany) prior to adding appropriate aliquots to the AP1 medium for the  
92 biomineralization experiments to achieve final concentrations of 10 and 20 mM FeSO<sub>4</sub>. All  
93 experiments were conducted at least in triplicate.

94

### 95 **2.3 Preparation of nZVI/fungal biomass composite**

96 To prepare the nano zerovalent iron (nZVI)/fungal biomass composite, fungal biomass was  
97 collected after 6 d incubation in Fe-modified AP1 medium by centrifugation (4770 g x 20 min,  
98 4°C), washed with Milli-Q water and dried in a vacuum freeze dryer (JOYN FD-1C-50,  
99 Shanghai, China) for several hours. The dried biomass was ground to a fine powder using an  
100 agate mortar and pestle and then put into a quartz boat. Carbonization of fungal biomass and  
101 the reduction of Fe<sup>2+</sup> to Fe<sup>0</sup> were achieved by increasing the temperature to 900°C in a tube  
102 furnace (KejingOTF-1200X, Hefei, China) at a heating rate of 5°C min<sup>-1</sup> which was then  
103 maintained for 1 h. Nitrogen gas was used to keep the atmosphere anaerobic during the whole  
104 process.

105

### 106 **2.4 Characterization of minerals precipitated by *N. crassa***

107 Samples were fixed using 2.5% glutaraldehyde in 5 mM PIPES buffer (pH = 6.5) for 24 h at  
108 room temperature and then washed twice using the same PIPES buffer. Dehydration was

109 performed using vacuum freeze drying (SCIENTZ-10YG/A, Ningbo, China). Morphological  
110 and elemental analysis of fungal biomass before and after heat treatment were conducted using  
111 scanning electron microscopy (SEM) (ZEISS Gemini 300, Oberkochen, Germany) and energy  
112 dispersive X-ray analysis (EDXA) operating at voltages of 15 kV and 20 kV, respectively. The  
113 identification of biominerals was carried out using X-ray diffraction (XRD) (Bruker D8  
114 Advance, Karlsruhe, Germany), Fourier transform infrared spectroscopy (FTIR) (Thermo  
115 Fisher 6700, Waltham, USA) and X-ray photoelectron spectroscopy (XPS) (Thermo Fisher,  
116 Waltham, MA, USA). Sample preparation and curve fitting analysis were conducted according  
117 to the procedures described in Li et al. [23].

118 After carbonization and reduction of  $\text{Fe}^{2+}$ , the surface properties and surface area of fungal  
119 biomass and the biogenic nZVI/fungal biomass composite were characterized by  $\text{N}_2$   
120 adsorption/desorption measurements using a surface area analyzer (Micromeritics ASAP 2020  
121 HD88, Norcross, GA, USA). The thermal stability of the sample was investigated using  
122 thermogravimetric analysis-differential scanning calorimetry (TGA-DSC) (SDT Q600 V20.9  
123 Build 20, TA instruments, DE, USA) in a nitrogen atmosphere ( $100 \text{ ml min}^{-1}$ ) from room  
124 temperature to  $900^\circ\text{C}$  at a rate of  $5^\circ\text{C min}^{-1}$ .

125 A 2 ml sample, from a 10% (w/v) solution in 10 ml MilliQ water, after heat treatment, was  
126 examined for stability using a LUMiSizer Dispersion Analyser (LUM GmbH, Berlin,  
127 Germany). The wavenumber for the space and time resolved extinction profiles (STEPTM)  
128 was 865 nm and the sedimentation speed was 4000 rpm. The transmitted light detector was  
129 used to scan along the height of the synthetic sample cell for 1 h.

130

### 131 **2.5 Removal of carbon tetrachloride from solution by the ‘iron coral’ composite**

132 For the degradation experiments, 0.1 g of biogenic nZVI/fungal biomass composite was added  
133 to 100 ml  $\text{CCl}_4$  solution ( $16 \text{ mg l}^{-1}$ , first dissolved in methanol) and kept in a shaking incubator

134 (125 rpm, 25°C) for 150 min. The concentration of CCl<sub>4</sub> and the intermediate degradation  
135 products were measured every 30 min using a gas chromatography-mass spectrometer (GC-  
136 MS) (7890B-5977A, Agilent Technologies, CA, USA), and the selected ion monitoring (SIM)  
137 method of quantitation was selected.

138

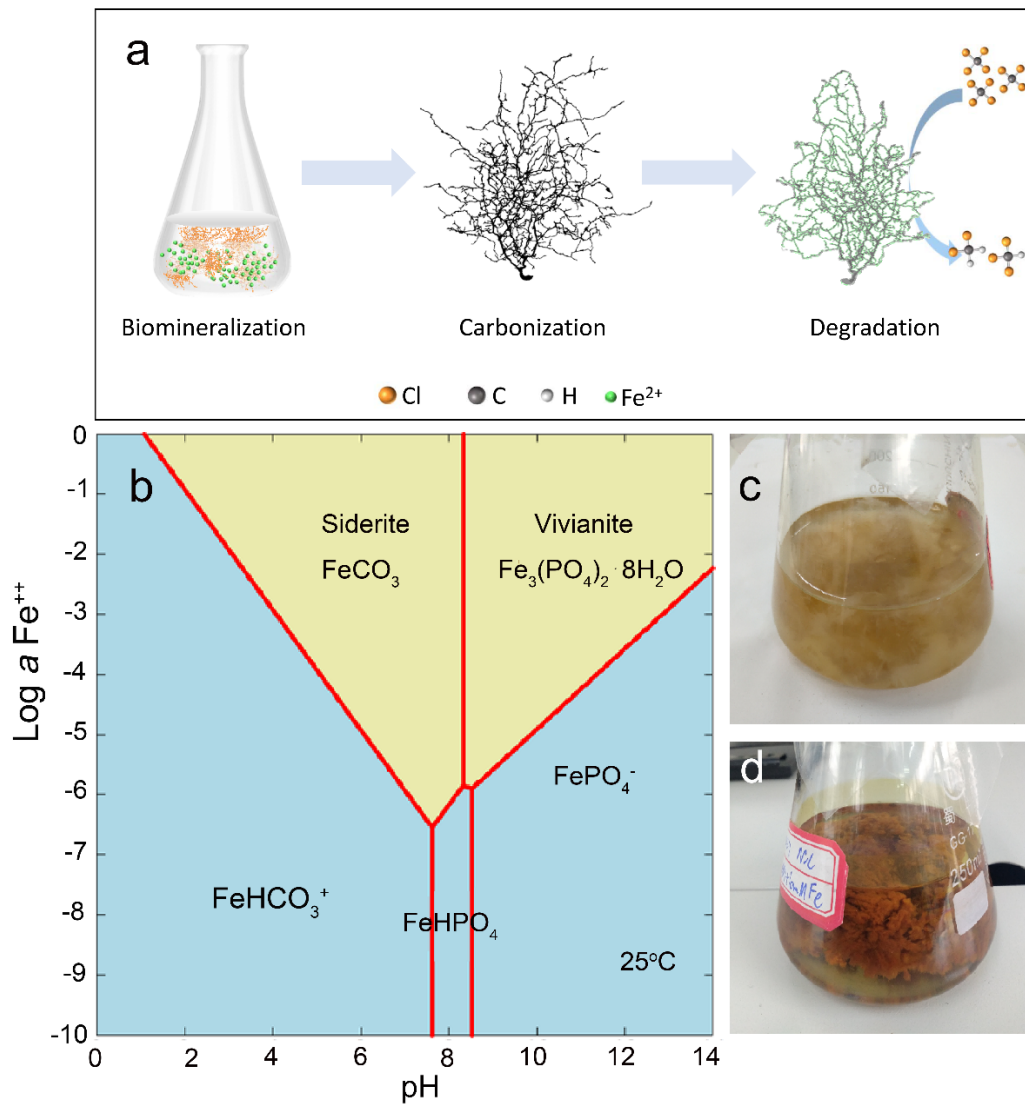
## 139 **2.6 Tafel scans of the ‘iron coral’ composite and commercial nZVI**

140 To investigate the ability of iron coral to lose electrons, Tafel scans were performed on a CHI-  
141 660E electrochemical workstation fitted with a three electrode system enabling the free  
142 corrosion potentials to be recorded. Sample preparation was conducted according to the  
143 procedures described in Hu et al. [25].

144 **3. Results**

145 **3.1 Characterization of the biogenic nZVI/fungal biomass composite ‘iron coral’**

146 The preparation of the biogenic nZVI/fungal biomass composite is illustrated in Fig. 1a. The  
147 ureolytic fungus was incubated in Fe-modified media to achieve biomineralization of Fe-  
148 containing minerals, followed by carbonization to obtain the biogenic nZVI/fungal biomass  
149 composite, which was subsequently applied for the degradation of CCl<sub>4</sub>. The solubility and  
150 stability of Fe<sup>2+</sup>, relevant Fe-containing minerals, and the predominance of aqueous Fe species  
151 were calculated individually in a simulated fungal growth supernatant system using GWB. The  
152 obtained results showed that siderite (FeCO<sub>3</sub>) and vivianite (Fe<sub>3</sub>(PO<sub>4</sub>)<sub>2</sub>·8H<sub>2</sub>O) were the main  
153 minerals in the simulated medium (Fig. 1b). Iron carbonate (FeCO<sub>3</sub>) could precipitate over a  
154 range of pH 1 to 8.3 while the lowest concentration of Fe<sup>2+</sup> for carbonate precipitation was  
155 around 0.32 μM (here,  $a(\text{Fe}^{2+})$  was equal to Fe<sup>2+</sup> concentration,  $\log a(\text{Fe}^{2+}) \approx -6.5$ ,  $c(\text{Fe}^{2+}) \approx$   
156  $a(\text{Fe}^{2+}) \approx 0.32 \mu\text{M}$ ).

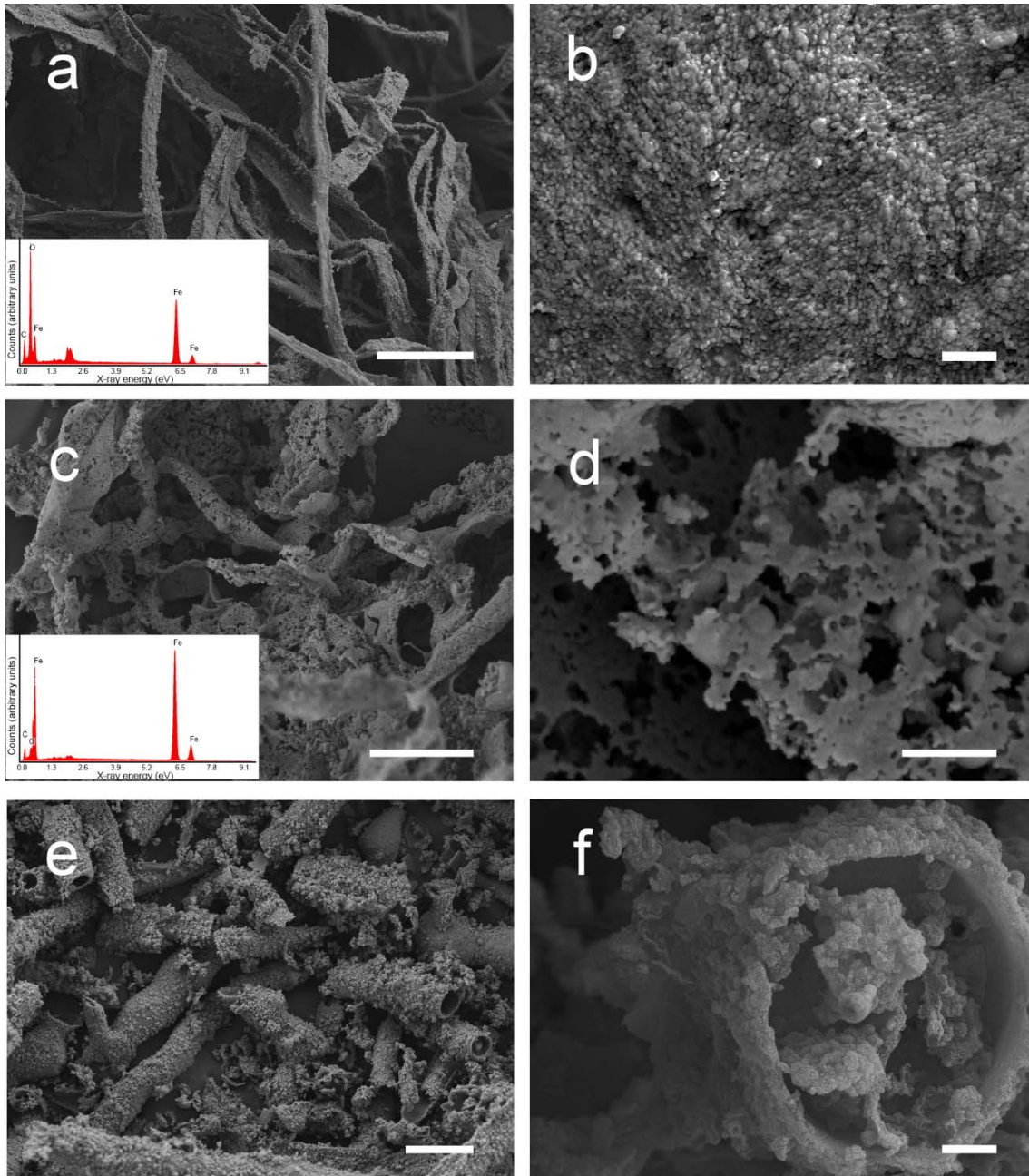


157

158 **Figure 1.** (a) Schematic illustration of the synthesis of nano zerovalent iron with a unique N-  
 159 doped branching structure. (b) Solubility diagram of Fe<sup>2+</sup> versus pH at 25°C in a geochemically  
 160 simulated medium containing 0.33 M CO<sub>3</sub><sup>2-</sup> after incubation with *N. crassa*. Chemical  
 161 parameters of the simulated system were set at 0.33 M CO<sub>3</sub><sup>2-</sup>, 6.1 mM Cl<sup>-</sup>, 0.83 mM SO<sub>4</sub><sup>2-</sup>, 0.66  
 162 M NH<sub>4</sub><sup>+</sup>, 4 mM K<sup>+</sup>, 0.8 mM Mg<sup>2+</sup>, 1.7 mM Na<sup>+</sup>, 0.2 mM Ca<sup>2+</sup>, 0.02 mM Mn<sup>2+</sup>, 0.01 Mm Zn<sup>2+</sup>  
 163 and 9 μm Fe<sup>3+</sup>. The symbol *a* on the y-axis represents the effective concentration of a given  
 164 chemical species in a mixture. (c) Images of *N. crassa* grown in control AP1 liquid medium or  
 165 (d) AP1 containing 10 mM Fe<sup>2+</sup> for 6 d at 25°C in the dark. Typical images are shown from  
 166 many similar examples.

167 After 6 d incubation, fungal biomass in control medium was pale yellow and flocculent (cotton  
168 wool-like) (Fig. 1c) while in Fe-modified AP1 medium, the fungal biomass tended to aggregate  
169 and yellow minerals were precipitated around the hyphae as well as in the medium (Fig. 1d),  
170 the colour changes clearly visible to the naked eye. The SEM results showed that the fungal  
171 hyphae were enveloped by a compact layer of minerals (Fig. 2a). This mineral sheath was  
172 comprised of granular nanoscale particles (~80 nm) (Fig. 2b) and the main elements detected  
173 in the minerals were C, O and Fe (Fig. 2a) which suggested formation of iron carbonates and  
174 oxides according to previous experiments [22].

175 After the carbonization and reduction process (heat treatment at 900°C), the surface of the  
176 fungal hyphae became porous with individual nanoparticles (~50 nm) adhering to the  
177 carbonized hyphae, resulting in a coralline appearance, for which we designated the epithet  
178 'iron coral' (Fig. 2c, d). EDXA analysis showed that C and Fe were the main elements in the  
179 'iron coral' and little O was detected (Fig. 2c). At the higher concentration of Fe<sup>2+</sup> (20 mM),  
180 more minerals were precipitated around the hyphae and after the heat treatment, the Fe-  
181 containing mineral sheath was still compact (Fig. 2e,f) but the mineral particles attached to the  
182 hyphae were larger (200~300 nm) than those forming at the lower concentration of Fe<sup>2+</sup> (10  
183 mM) (Fig. 2d,f). To further confirm the location and distribution of iron within the biominerals  
184 after heat treatment, X-ray mapping was carried out. It was found that iron was distributed  
185 evenly around the carbonized fungal hyphae (Fig. S1). Simple qualitative analysis from EDXA  
186 estimated that the amount of Fe was around 40% while carbon and oxygen were 45% and 15%,  
187 respectively.

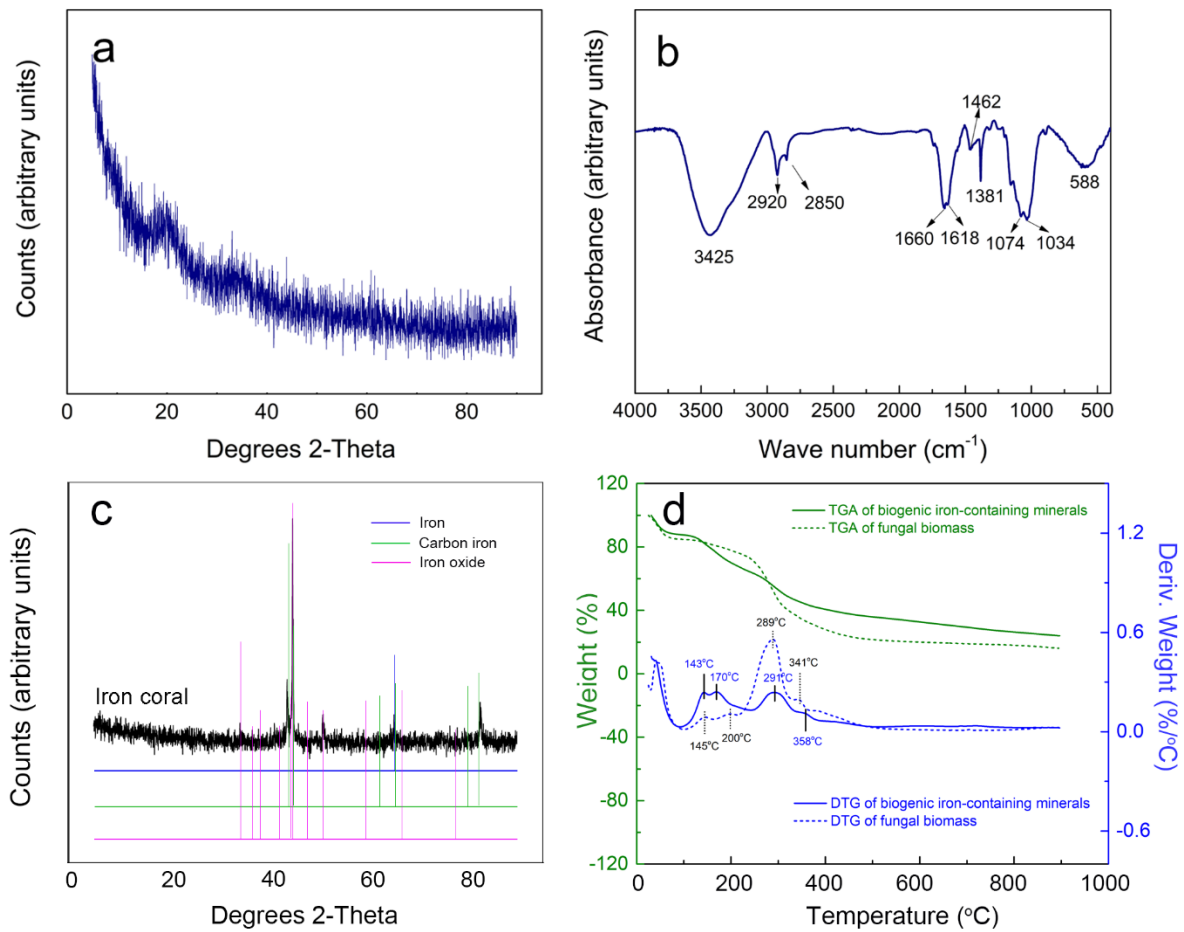


188

189 **Figure 2.** Scanning electron microscopy (SEM) and elemental analysis of minerals precipitated  
 190 by *N. crassa* in Fe-modified media. Images are (a, b, e) before and (c, d, f) after biomass  
 191 carbonization at 900°C under nitrogen gas for 1 h. Insets show X-ray energy dispersive analysis  
 192 (EDXA) of the minerals precipitated by *N. crassa* (a) before and (c) after carbonization. Scale  
 193 bars: (a) = 20 μm, (b, d) = 400 nm, (c, e) = 10 μm, (f) = 600 nm. *N. crassa* was incubated with  
 194 (a-d) 10 mM, or (e, f) 20 mM Fe<sup>2+</sup> for 12 d at 25°C in the dark. Typical images and spectra are  
 195 shown from many similar examples.

196 XRD showed that minerals precipitated by *N. crassa* grown in Fe-modified medium were  
197 amorphous (Fig. 3a), precluding accurate identification, which might be due to the  
198 bioprecipitation process being influenced by extracellular metabolites (e.g. protein, peptides,  
199 polysaccharide, amino acids) [23]. FTIR spectroscopy was further applied for identification of  
200 the biominerals precipitated (Fig. 3b). The broad absorption band at  $3425\text{ cm}^{-1}$  was related to  
201 the O-H stretching vibrations arising from hydroxyl groups in water. The bands at 2920 and  
202  $2850\text{ cm}^{-1}$  were due to C-H stretching corresponding to organic matter [26] in biomass.  
203 Previous experiments have demonstrated that peaks in the region of  $1660$  to  $1381\text{ cm}^{-1}$  were  
204 attributable to the  $\nu_3$  vibrational mode of the carbonate ion, while the peaks at 1074 and 1034  
205  $\text{cm}^{-1}$  are due to the  $\nu_1$  vibrational mode of  $\text{CO}_3^{2-}$ . The adsorption band at  $588\text{ cm}^{-1}$  can be  
206 assigned to the vibrations of Fe-O which refers to iron oxide [27, 28]. Compared with the  
207 EDXA results, it can be concluded that the biominerals precipitated were a mixture of hydrated  
208 iron carbonate with trace amounts of iron oxides and ferric hydroxide (the latter according to  
209 the medium colour) which was consistent with the geochemical simulation results. After the  
210  $900^\circ\text{C}$  heat treatment under a nitrogen atmosphere, the composite of fungal biomass and iron-  
211 containing minerals (from medium containing 10 mM Fe) was identified as a mixture of  
212 zerovalent iron ( $\text{Fe}^0$ ), carbon iron ( $\text{Fe}_{1.91}\text{C}_{0.09}$ ) and iron oxide ( $\text{Fe}_3\text{O}_4$ ) (Fig.3c) which was  
213 consistent with the EDXA results (Fig. 2c). Therefore, after heat treatment, a mixture of  
214 carbonized fungal biomass with nanoscale zerovalent iron ('iron coral') was achieved. The  
215 existence of trace amount of oxides might due to the subsequent oxidation of  $\text{Fe}^0$  on the surface.  
216 To further investigate the formation process of 'iron coral', TGA was applied to analyse the  
217 thermal stability of prepared biogenic iron-containing minerals and fungal biomass before heat  
218 treatment (Fig. 3d). The main weight loss for fungal biomass and biogenic iron-containing  
219 minerals below  $120^\circ\text{C}$  can be attributed to the release of free water or structural water [29].  
220 There were several thermal events occurring from  $140$ - $300^\circ\text{C}$  which corresponded to

221 crystallization from the amorphous phase and subsequent decomposition of carbonates to  
 222 oxides (Fig.3a, c). The peak at 358°C could be assigned to reduction of the iron oxide to  
 223 zerovalent iron which was verified by the XRD results (Fig. 3c). For the fungal biomass, a  
 224 series of events occurred with increasing temperature and the biomass dehydrated (below  
 225 130°C) and then carbonized gradually from 130 to 341°C.



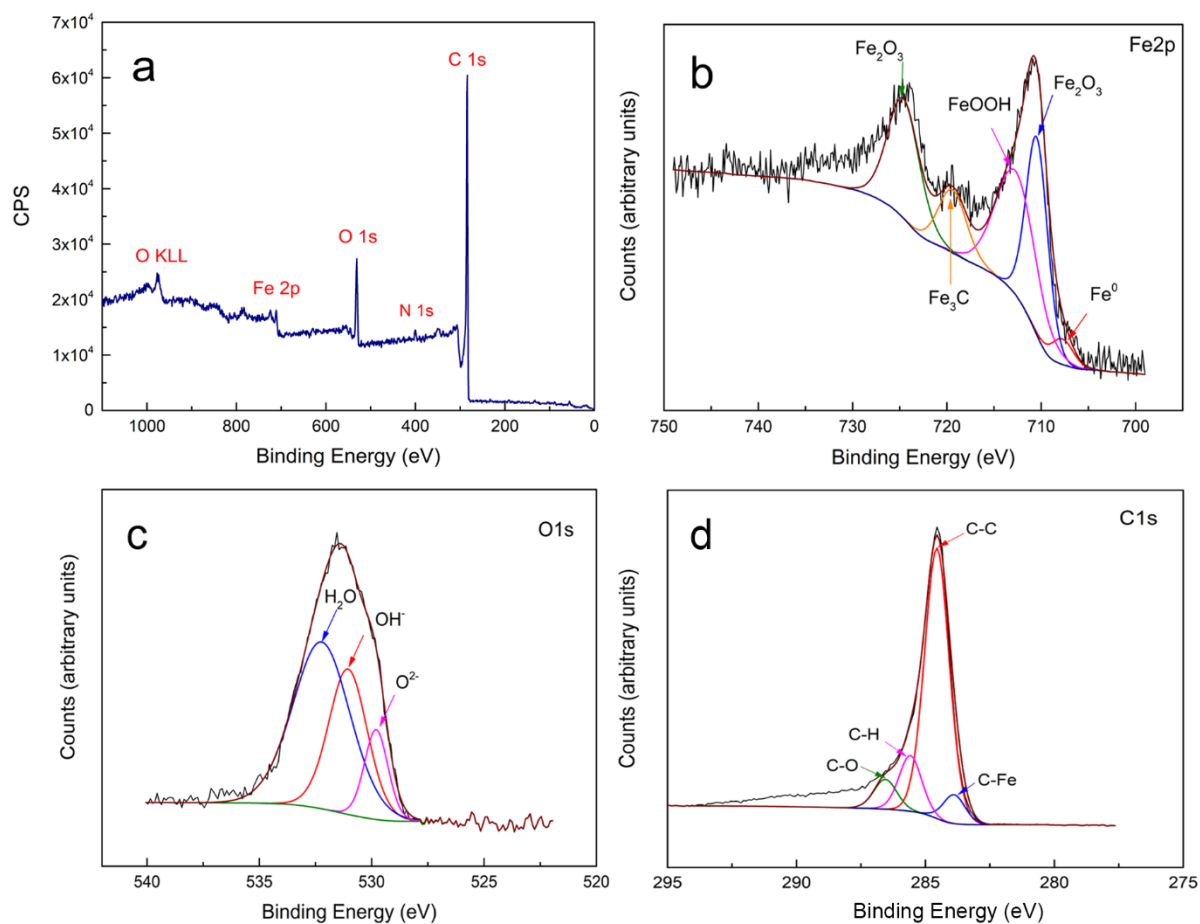
226  
 227 **Figure 3.** Characteristics of minerals precipitated by *N. crassa*. (a) X-ray diffraction (XRD)  
 228 and (b) infrared spectroscopy (IR) of iron-containing minerals precipitated before  
 229 carbonization and iron reduction. (c) XRD of minerals precipitated by *N. crassa* after  
 230 carbonization and reduction at 900°C for 1 h. *N. crassa* was cultured in AP1 liquid medium  
 231 amended with 10 mM Fe<sup>2+</sup> for 6 d at 25°C in the dark. (d) Thermogravimetric analysis (TGA)  
 232 and derivative thermogravimetric (DTG) curves of biogenic iron-containing minerals and  
 233 fungal biomass under nitrogen at a heating rate of 5°C min<sup>-1</sup>. Green and blue lines refer to TGA

234 and DTG, respectively. Solid and dashed lines are for iron-containing minerals and fungal  
235 biomass, respectively. Typical patterns and curves are shown from one of several  
236 determinations.

237

238 XPS was employed to investigate the surface chemical properties of 'iron coral'. The fully  
239 scanned spectrum of the sample showed five main peaks, at 977.1 eV, 716.3 eV, 530.7 eV, 400  
240 eV and 283.9 eV, corresponding to O KLL, Fe 2p, O 1s, N 1s and C 1s, respectively (Fig. 4a).  
241 Four characteristic peaks were identified in the Fe 2p region, and the XPS spectrum for Fe 2p<sub>3/2</sub>  
242 and Fe 2p<sub>1/2</sub> core levels showed binding energies of 724.6 eV and 710.5 eV, respectively, which  
243 refer to Fe<sub>2</sub>O<sub>3</sub> [30-32] (Fig. 4b). The peaks at 719.4 and 707.8 eV indicated the presence of  
244 carbon iron and elemental iron (Fe<sup>0</sup>) on the surface, respectively [30]. The peak at 712.7 eV  
245 represents the oxidized state of FeOOH.[32, 33]. The O 1s spectrum fitted with three  
246 components at 529.8, 531.1 and 532.2 eV, which correspond to oxide oxygen, hydroxyl groups  
247 and adsorbed water, respectively.[30, 32] (Fig. 4c). The presence of iron oxide suggested that  
248 the freshly prepared nano zerovalent iron was still partially oxidized. The XPS C 1s spectrum  
249 could be deconvoluted into four components, including C-Fe (283.8 eV), C-C (284.5 eV), C-  
250 H (285.6 eV), and C-O (286.6 eV) [28, 34] (Fig. 4d).

251 Pore size distributions of the carbonized fungal biomass and 'iron coral' composite were  
252 evaluated through N<sub>2</sub> adsorption/desorption isotherms (Fig. S2). Both samples exhibited a type  
253 IV isotherm with type H4 hysteresis loops, indicating a typical microporous and mesoporous  
254 structure in accordance with the IUPAC classification [30, 35]. The BET surface area of  
255 carbonized fungal biomass and iron coral were calculated to be 289.3 and 160.4 m<sup>2</sup> g<sup>-1</sup>,  
256 respectively. In terms of pore size distribution, both carbonized fungal biomass and 'iron coral'  
257 displayed a multimodal pore size distribution with the pore sizes being less than 100 nm  
258 diameter.



260

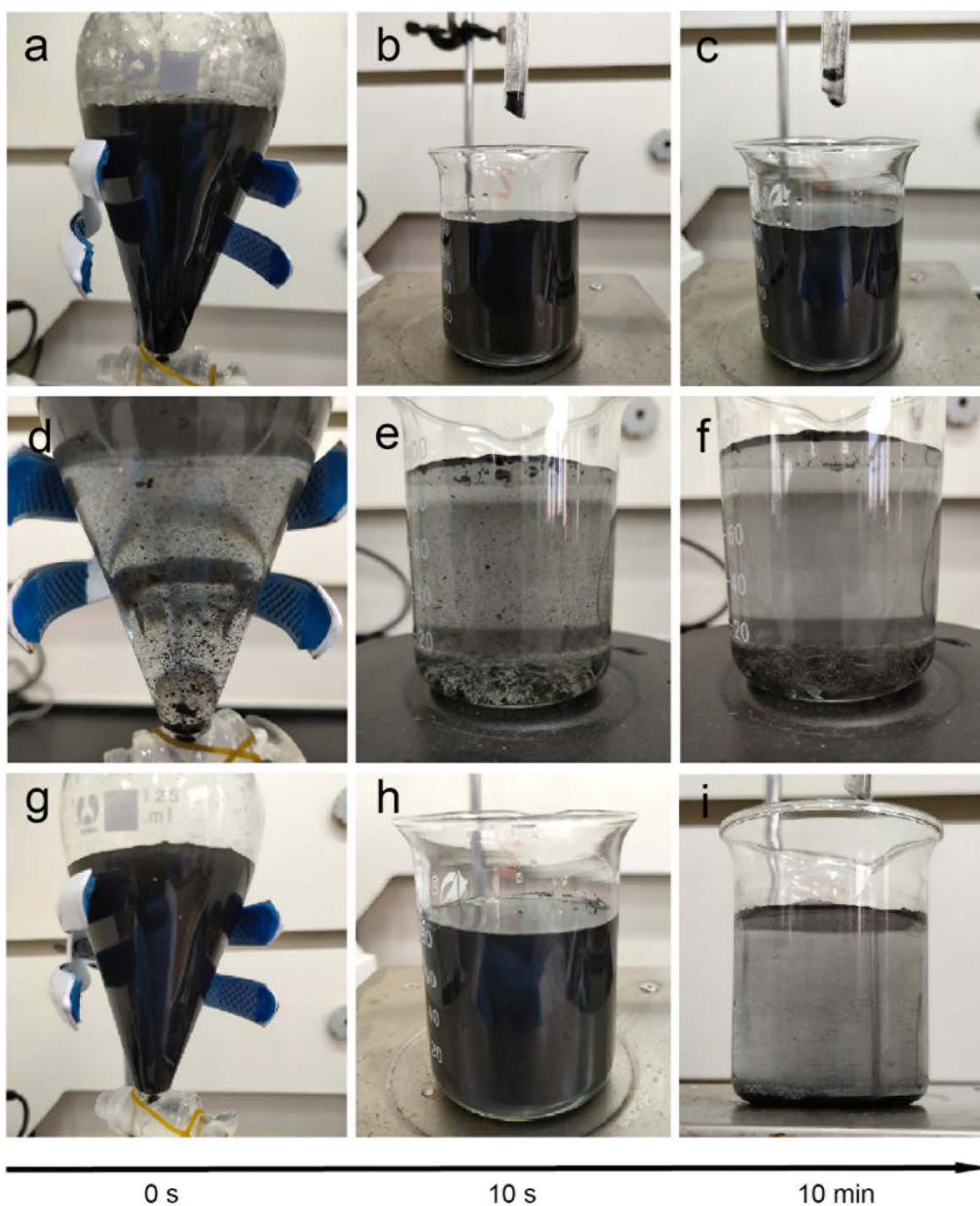
261 **Figure 4.** (a) X-ray photoelectron spectroscopy (XPS) survey spectrum for the ‘iron coral’  
 262 composite and high resolution XPS spectra of (b) Fe 2p, (c) O 1s and (d) C 1s. A typical pattern  
 263 and spectra are shown from one of several determinations.

264

### 265 3.2 Stability of the iron coral composite

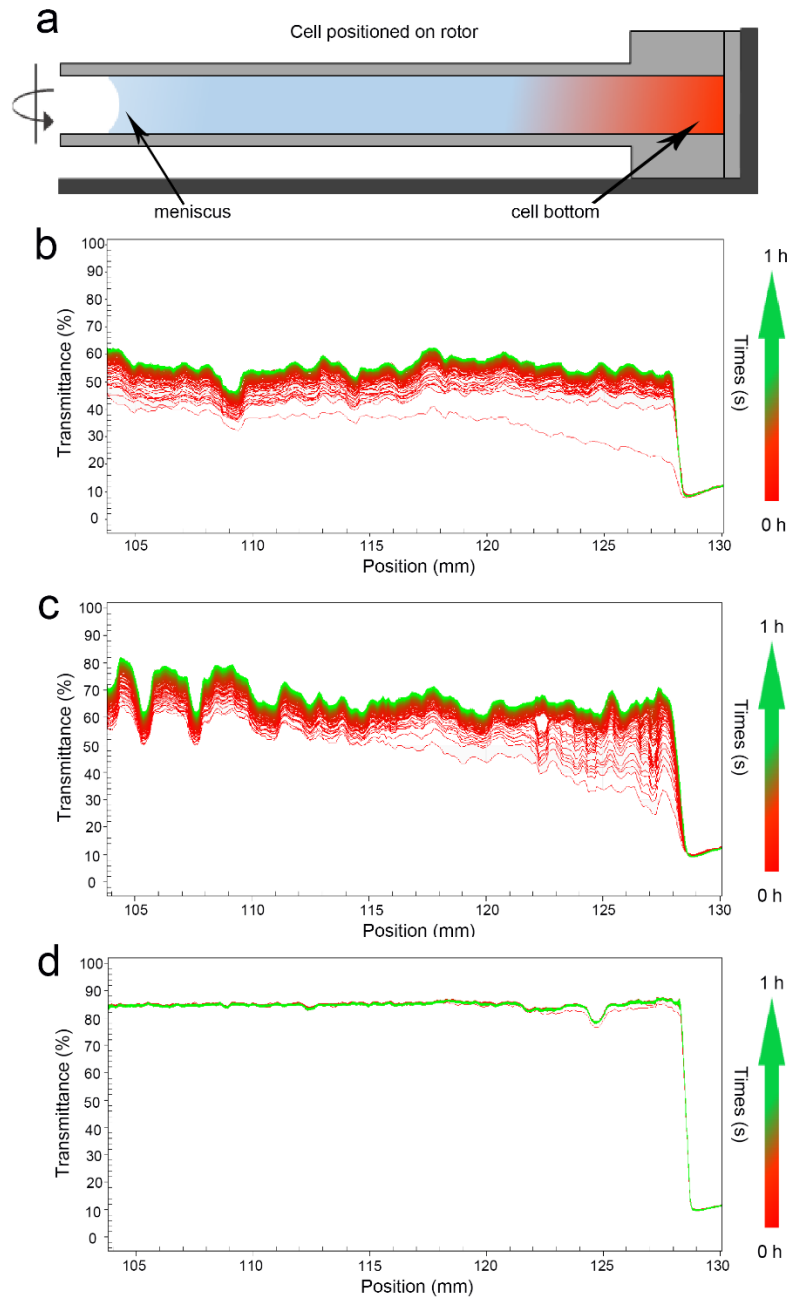
266 The migration of biomineralized iron coral in an aqueous solution was conducted to evaluate  
 267 stability (Fig. 5a, d, g) and the zeta potential measurements for iron coral are shown in [Fig.S3](#).  
 268 Once mixed with water, the carbonized fungal biomass dispersed into different layers due to  
 269 weight differences while the iron coral composite and commercial nZVI distributed evenly in  
 270 the solution within the first 10 s (Fig. 5b, e, h). However, both the carbonized fungal biomass  
 271 and commercial nZVI subsequently settled with the solution clearing and becoming transparent

272 while the solution containing ‘iron coral’ remained dark (Fig. 5c, f, i) which illustrated its  
273 nanoparticulate nature, and properties of enhanced mobility and dispersability. To further  
274 investigate the stability and mobility of the iron coral composite, stability analysis was applied  
275 using a LUMi X-Ray Reader during the sedimentation process (Fig. 6). The different coloured  
276 curves represent the intensity of transmitted light from the meniscus to the vessel bottom at  
277 selected time intervals. The first red line at the bottom represents the intensity of transmitted  
278 light over the first 10 s. Except for the cell bottom, the transmitted light intensity of the cell  
279 with iron coral (Fig. 6b) and fungal biomass (Fig. 6c) increased gradually within 1 h (Fig. 6b).  
280 The sedimentation process of the iron coral composite was more stable and the transmitted  
281 light increased gradually from 45% to 60% (except over the first 10 s). For the fungal biomass,  
282 the sedimentation behaviour depended on its position: the sedimentation rate of the sample in  
283 the upper layer of the cell was rapid while the sample in the lower layer sedimented slowly  
284 (Fig. 6c) which may be due to size differences in the fungal biomass. The intensity of the cell  
285 containing commercial nZVI (Fig. 6d) decreased significantly and blocked the transmitted light  
286 which indicated the rapid sedimentation of these particles. These results clearly showed that  
287 the stability of the iron coral composite in aqueous solution was better than fungal biomass  
288 alone and commercial nZVI particles.



289

290 **Figure 5.** Mobility of (a-c) iron coral composite, (d-f) carbonized fungal biomass and (g-i)  
 291 commercial nZVI in water at different time periods. The concentration of the solid materials  
 292 was  $1 \text{ g L}^{-1}$  (dry weight). Typical images are shown from many similar samples.



293

294 **Figure 6.** Evolution of time dependent transmission profiles of iron coral, zerovalent iron or  
 295 fungal biomass suspension. (a) Diagram of the measurement principle of the Stability Analyser.  
 296 (b) iron coral composite, (c) carbonized fungal biomass, (d) commercial nano zerovalent iron.  
 297 Different coloured curves represent the intensity of transmitted light from the meniscus to the  
 298 bottom of the vessel at different scan times. Profiles were taken every 10 s at 1000 rpm over 1  
 299 h.

### 300 3.3 Removal of carbon tetrachloride by iron coral

301 The performance of iron coral (obtained using 10 mM Fe<sup>2+</sup>), carbonized fungal biomass and  
 302 commercial nZVI was evaluated for the removal of carbon tetrachloride (CCl<sub>4</sub>) from aqueous  
 303 solution. The three solid sample materials (0.1 g) were mixed with CCl<sub>4</sub> (16 mg L<sup>-1</sup>) and the  
 304 concentration of CCl<sub>4</sub> in solution was measured at 30 min intervals. After 150 min reaction,  
 305 the concentration of CCl<sub>4</sub> decreased to different levels: the iron coral composite showed the  
 306 highest removal rate of around 75% while only 40% of CCl<sub>4</sub> was removed by carbonized fungal  
 307 biomass and 66% of CCl<sub>4</sub> was removed by commercial nZVI (Table 1). To further investigate  
 308 the intermediate degradation products during the reaction with iron coral, the aqueous solution  
 309 was analyzed at 30 min intervals. It was found that the main product detected was CCl<sub>4</sub> with  
 310 trace dichloromethane (CH<sub>2</sub>Cl<sub>2</sub>) and little trichloromethane (CHCl<sub>3</sub>) being detected (Fig. 7a).  
 311 Concomitant with the decrease of CCl<sub>4</sub> in solution, the amount of CH<sub>2</sub>Cl<sub>2</sub> increased gradually  
 312 with time (Fig.7b-d). The concentration of Cl<sup>-</sup> in the aqueous solution also increased with time  
 313 (data not shown).

314  
 315 **Table 1** Concentrations of CCl<sub>4</sub> in solution after reaction with iron coral, carbonized fungal  
 316 biomass or commercial nZVI.

	Concentration of CCl <sub>4</sub> (mg l <sup>-1</sup> ) in solution after different reaction times (min)						Proportion of CCl <sub>4</sub> removed (%)
	0	30	60	90	120	150	
Iron coral composite	10.77±0.00	6.18±0.69	5.21±0.98	3.33±0.39	3.60±0.20	2.73±0.30	74.7
Carbonized fungal biomass	10.77±0.00	13.72±3.07	10.26±2.90	7.16±1.07	7.53±1.09	6.45±0.52	40.1
Commercial nZVI	11.67±0.00	10.34±2.03	9.71 ± 0.47	7.40±0.87	5.50±0.64	3.97±0.03	66.0

317

318 To further investigate the degradation kinetics of CCl<sub>4</sub> by iron coral, the concentrations of CCl<sub>4</sub>  
319 in solution over reaction time were analyzed, the blue dots showing the experimental data and  
320 the red line representing the simulated data (Fig. 7e). The results showed that the kinetics of  
321 degradation by iron coral can be described as a pseudo-first-order kinetic reaction (eq. 1.1):

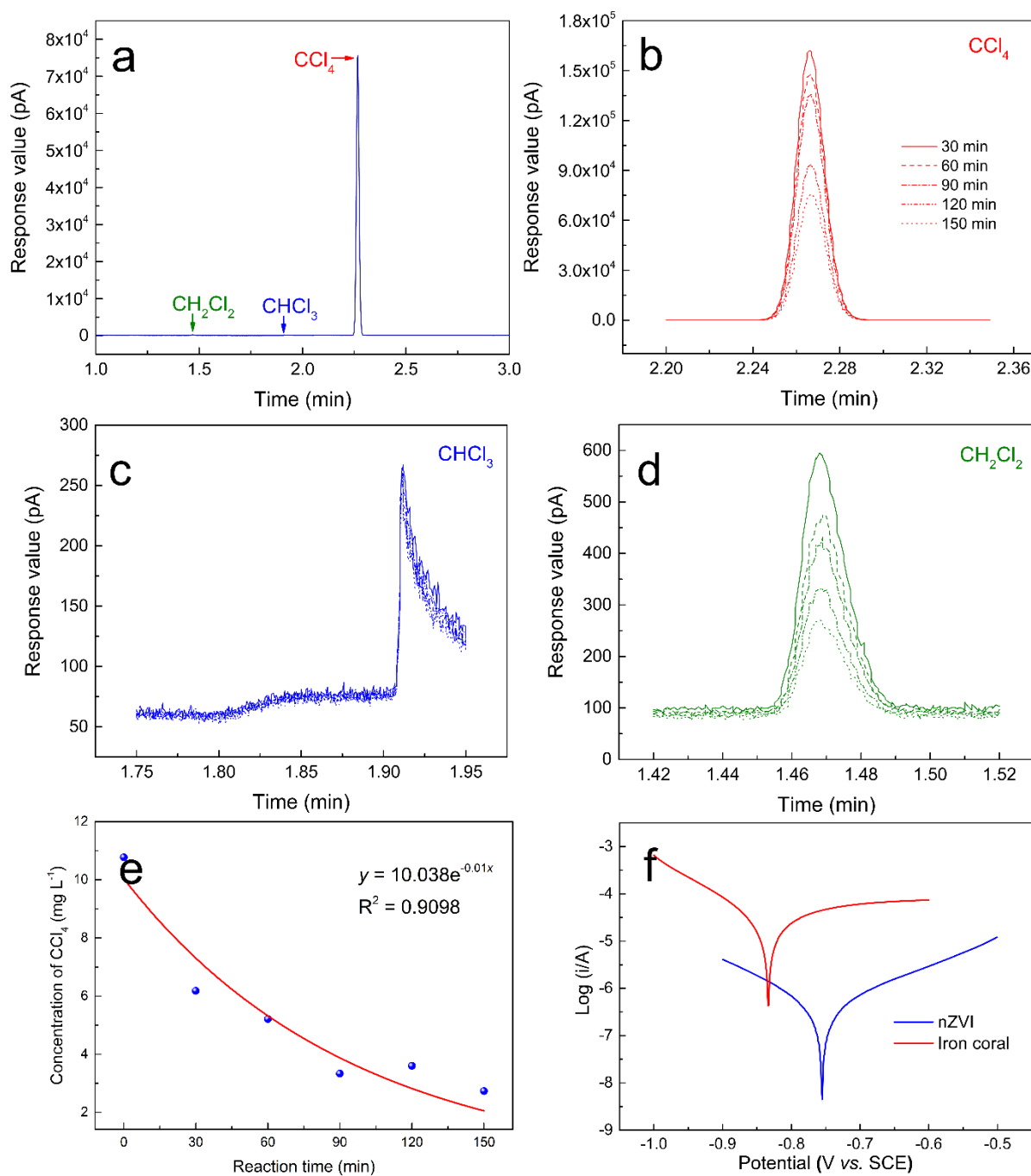
$$322 \quad \ln(C_t/C_0) = -k_{obs} t \quad (1.1)$$

$$323 \quad y = C_0 e^{-k_{obs}x} \quad (1.2)$$

$$324 \quad y = 10.038 e^{-0.01x} \quad (1.3)$$

325 Here,  $C_t$  was the concentration of CCl<sub>4</sub> remaining in solution after reaction,  $C_0$  is the initial  
326 concentration of CCl<sub>4</sub> in the simulated model,  $k_{obs}$  is the first-order rate constant and  $t$  is the  
327 reaction time. The relation between the concentration of CCl<sub>4</sub> remaining in solution ( $y$ ) and  
328 reaction time ( $x$ ) can be described by equation 1.2 in Fig. 7e. In this experiment, the initial  
329 concentration of CCl<sub>4</sub> in the simulated model was calculated as 10.038 mg L<sup>-1</sup>,  $k_{obs}$  was -0.01  
330 and R<sup>2</sup> was 0.9098 (eq.1.3), which shows that the experimental data fitted very well with the  
331 simulated model and the degradation kinetics of CCl<sub>4</sub> followed a pseudo-first-order model.

332 To unravel the reasons for the CCl<sub>4</sub> degradation ability of iron coral, the electron transfer  
333 properties of iron coral were checked using a Tafel scan technique which was used to measure  
334 free corrosion potentials (Fig. 7f). The results showed that the free corrosion potentials for iron  
335 coral and commercial nZVI were -0.76 and -0.84 V, respectively. The lower free corrosion  
336 potential of the sample is easily recognized to reflect corrosion, which indicates a higher ability  
337 to lose electrons. This 80 mV gap in the free corrosion potentials between iron coral and  
338 commercial nZVI suggested that electron release from iron coral was faster than that from  
339 commercial nZVI, and this contributed to the superior CCl<sub>4</sub> degradation performance of the  
340 iron coral.



341

342 **Figure 7.** Formation of degradation products in solution over reaction time with iron coral. (a)  
 343 Products detected after 50 min and changes in the relative amounts of (b)  $\text{CCl}_4$ , (c)  $\text{CHCl}_3$ , (d)  
 344  $\text{CH}_2\text{Cl}_2$  in solution according to changes in peak intensity. (e) Kinetics of  $\text{CCl}_4$  degradation by  
 345 the iron coral composite and (f) Tafel scans of iron coral and commercial nZVI in  $0.5 \text{ mol L}^{-1}$   
 346  $\text{NaSO}_4$  solution. Typical chromatograms are shown from one of several determinations.

#### 4. Discussion

Nanosized zerovalent iron nZVI has been widely investigated for the remediation or reductive dechlorination of chlorinated solvents from contaminated sites due to its high reactivity with contaminants and mobility in porous media [36-38]. However, the major technical challenge for preparing nZVI particles is to prevent aggregation and develop stabilized nZVI through appropriate surface modification technology and/or creating a network with an additional stabilizer (e.g. polymers, surfactants, silica) that separates the nanoparticles [39]. Not all those methods are applicable for preparation of nZVI and some polymers may not function properly in the aqueous phase while some stabilizers may cause secondary contamination. In this research, a fungal biomineralization process was used for the synthesis of nZVI. The biogenic nZVI distributed evenly around the fungal hyphae which we have termed 'iron coral' according to the morphology and the precipitation process. The biogenic iron coral showed an excellent removal capacity for CCl<sub>4</sub> (~75%) compared with carbonized fungal biomass or a commercial nZVI product.

Previous research has demonstrated that ureolytic fungi grown in urea-modified medium provide a promising method for the biomineralization of metal-containing minerals including carbonates, e.g. CaCO<sub>3</sub>, SrCO<sub>3</sub>, MnCO<sub>3</sub>, and oxides (MnO, Mn<sub>2</sub>O<sub>3</sub>), especially those in the nanoscale [18, 19, 23]. The process of biomineralization refers to the formation of minerals by organisms and the final products may contain both minerals and organic components. Biomineralization processes include biologically-induced mineralization (BIM) and biologically-controlled mineralization (BCM). The formation of a coral skeleton is representative of BCM, which can be described as a protein controlling the process of mineral crystallization with the organic matrix controlling and influencing the biomineralization process and end-stage densification [40]. For the BIM process, e.g. ureolytic fungi incubated in urea and Fe<sup>2+</sup>-supplemented medium, degradation of urea and the release of carbonate

increases the pH of the microenvironment, and results in the precipitation of iron carbonate.

The geochemical simulation of iron and carbonate speciation in the reaction system matched very well with the experimental data. The filamentous hyphae were surrounded by iron-containing minerals and after heat treatment, the iron nanoparticles (derived from the reduction of iron oxide by fungal biomass carbonization) were distributed evenly around the carbonized hyphae which resembled coral decorated with iron particles. Previous research has demonstrated that the conformation of extracellular proteins can play an important role in the fungal precipitation of nanoscale minerals [23], which is analogous to the formation of natural coral, hence 'iron coral'. Compared with carbonized fungal biomass, the BET surface area of biogenic iron coral was lower ( $160.4 \text{ m}^2 \text{ g}^{-1}$ ) which may be due to the nZVI being embedded in the fungal biomass and blocking the porous structure. This is consistent with findings for a nZVI synthesised through the reduction of  $\text{Fe}^{3+}$  by  $\text{NaBH}_4$  solution and supported by reductive graphene oxides [41].

The stability of the iron coral composite was much better than the carbonized fungal biomass and commercial nZVI. Stability is one of the most important factors determining degradation ability in the aqueous phase. When mixed with  $\text{CCl}_4$  solution ( $16 \text{ mg L}^{-1}$ ), little sedimentation occurred in the mixture containing the iron coral composite, which may be one of the reasons that the iron coral composite showed higher  $\text{CCl}_4$  degradation ability (75%) than that of carbonized fungal biomass and commercial nZVI. Some previous research has been carried out on the degradation of chlorinated organic compounds by nZVI. Formic acid was applied to enhance the degradation of  $\text{CCl}_4$  ( $2 \text{ mg L}^{-1}$ ) by nZVI and the degradation efficiency increased from 11.4% to 85% [42], while the  $\text{CCl}_4$  ( $2 \text{ mg L}^{-1}$ ) removal efficiency of nZVI assembled on the surface of  $\text{Fe}_3\text{O}_4$  was around 66% [43]. Most of the obtained kinetic data fitted to a pseudo-first-order kinetic model [43-46]. Ma et al. [47] reported that 94% of  $\text{CCl}_4$  ( $3 \text{ mg L}^{-1}$ ) could be efficiently removed from aqueous solution by nanoscale palladized zero-valent iron-graphene

composites and that the degradation kinetics followed pseudo first-order reaction kinetics. Here, the dispersibility of nZVI was significantly improved by the graphene due to the larger specific surface area. In this experiment, the degradation kinetics of CCl<sub>4</sub> well fitted a pseudo-first-order reaction model, which was consistent with our reported findings. Moreover, the lower free corrosion potentials of iron coral composites (-0.84 V) indicated a higher ability to lose electrons, with the nitrogen in the fungal biomass inducing defects in the carbon framework which will also increase electron delocalization [48], thereby resulting in higher degradation of CCl<sub>4</sub>. This work shows that biogenic iron coral is an efficient and highly promising candidate for the removal of chlorinated hydrocarbon pollutants from aqueous solution. Furthermore, fungi are effective biosorbents for metal ions and the origin of Fe<sup>2+</sup> could be from, e.g. electroplating or mining wastewaters.

## 5. Conclusions

In this study, fungal biomineralization provided a facile method for the synthesis of nanoscale zerovalent iron (nZVI) showing a unique N-doped branching structure. Compared with commercial nZVI and carbonized fungal biomass, the iron coral composite showed excellent stability and mediated high degradation of carbon tetrachloride (~75%). The growth of ureolytic fungi in urea-containing media therefore provides a promising system for novel preparation of nZVI through a biomineralization process, with the iron coral nZVI/carbonized biomass showing significant potential for chlorinated pollutant removal from solution as well as metal recovery.

## Acknowledgments

This work was supported by the National Natural Science Foundation of China (Grant No.41701352); the Open Project Program of the State Key Laboratory of Petroleum Pollution

Control (Grant No. PPC2019012); and the National Key R&D Program of China (No. 2018YFC1801903-01). GMG gratefully acknowledges financial support of the Geomicrobiology Group from the Natural Environment Research Council, UK (NE/M010910/1 (TeaSe); NE/M011275/1 (COG<sup>3</sup>)).

## References

- [1] J. Yang, L. Meng, L. Guo, In situ remediation of chlorinated solvent-contaminated groundwater using ZVI/organic carbon amendment in China: field pilot test and full-scale application, *Environmental Science and Pollution Research* 25 (2018) 5051-5062.
- [2] M. Stefaniuk, P. Oleszczuk, Y.S. Ok, Review on nano zerovalent iron (nZVI): from synthesis to environmental applications, *Chemical Engineering Journal* 287 (2016) 618-632.
- [3] P. Wanner, B.L. Parker, S.W. Chapman, R. Aravena, D. Hunkeler, Quantification of degradation of chlorinated hydrocarbons in saturated low permeability sediments using compound-specific isotope analysis, *Environmental Science & Technology* 50 (2016) 5622-5630.
- [4] S. Chen, J. Bedia, H. Li, L.Y. Ren, F. Naluswata, C. Belver, Nanoscale zero-valent iron@mesoporous hydrated silica core-shell particles with enhanced dispersibility, transportability and degradation of chlorinated aliphatic hydrocarbons, *Chemical Engineering Journal* 343 (2018) 619-628.
- [5] X. Guan, Y. Sun, H. Qin, J. Li, I.M.C. Lo, D. He, H. Dong, The limitations of applying zero-valent iron technology in contaminants sequestration and the corresponding countermeasures: the development in zero-valent iron technology in the last two decades (1994–2014), *Water Research* 75 (2015) 224-248.
- [6] M. Mangayayam, K. Dideriksen, M. Ceccato, D.J. Tobler, The structure of sulfidized zero-valent iron by one-pot synthesis: impact on contaminant selectivity and long-term performance, *Environmental Science & Technology* 53 (2019) 4389-4396.
- [7] F. Fu, D.D. Dionysiou, H. Liu, The use of zero-valent iron for groundwater remediation and wastewater treatment: a review, *Journal of hazardous materials* 267 (2014) 194-205.
- [8] R. Mukherjee, R. Kumar, A. Sinha, Y. Lama, A.K. Saha, A review on synthesis, characterization, and applications of nano zero valent iron (nZVI) for environmental

- remediation, *Critical Reviews in Environmental Science and Technology* 46 (2016) 443-466.
- [9] H. Dong, Q. He, G. Zeng, L. Tang, C. Zhang, Y. Xie, Y. Zeng, F. Zhao, Y. Wu, Chromate removal by surface-modified nanoscale zero-valent iron: effect of different surface coatings and water chemistry, *Journal of colloid and interface science* 471 (2016) 7-13.
- [10] J. Soukupova, R. Zboril, I. Medrik, J. Filip, K. Safarova, R. Ledl, M. Mashlan, J. Nosek, M. Cernik, Highly concentrated, reactive and stable dispersion of zero-valent iron nanoparticles: direct surface modification and site application, *Chemical Engineering Journal* 262 (2015) 813-822.
- [11] R. Fu, Y. Yang, Z. Xu, X. Zhang, X. Guo, D. Bi, The removal of chromium (VI) and lead (II) from groundwater using sepiolite-supported nanoscale zero-valent iron (S-NZVI), *Chemosphere* 138 (2015) 726-734.
- [12] Y. Sun, C. Ding, W. Cheng, X. Wang, Simultaneous adsorption and reduction of U (VI) on reduced graphene oxide-supported nanoscale zerovalent iron, *Journal of Hazardous materials* 280 (2014) 399-408.
- [13] M.A. Kumar, S. Bae, S. Han, Y. Chang, W. Lee, Reductive dechlorination of trichloroethylene by polyvinylpyrrolidone stabilized nanoscale zerovalent iron particles with Ni, *Journal of Hazardous Materials* 340 (2017) 399-406.
- [14] Y. Zou, X. Wang, A. Khan, P. Wang, Y. Liu, A. Alsaedi, T. Hayat, X. Wang, Environmental remediation and application of nanoscale zero-valent iron and its composites for the removal of heavy metal ions: a review, *Environmental Science & Technology* 50 (2016) 7290-7304.
- [15] H. Chen, Y. Cao, E. Wei, T. Gong, Q. Xian, Facile synthesis of graphene nano zero-valent iron composites and their efficient removal of trichloronitromethane from drinking water, *Chemosphere* 146 (2016) 32-39.
- [16] M. Velimirovic, H. Chen, Q. Simons, L. Bastiaens, Reactivity recovery of guar gum coupled mZVI by means of enzymatic breakdown and rinsing, *Journal of Contaminant*

Hydrology 142 (2012) 1-10.

[17] Q.W. Li, L. Csetenyi, G.M. Gadd, Biomineralization of metal carbonates by *Neurospora crassa*, Environmental Science & Technology 48 (2014) 14409-14416.

[18] Q. Li, G.M. Gadd, Fungal nanoscale metal carbonates and production of electrochemical materials, Microbial Biotechnology 10 (2017) 1131-1136.

[19] Q. Li, L. Csetenyi, G.I. Paton, G.M. Gadd, CaCO<sub>3</sub> and SrCO<sub>3</sub> bioprecipitation by fungi isolated from calcareous soil, Environmental Microbiology 17 (2015) 3082-3097.

[20] G.M. Gadd, Geomicrobiology of the built environment, Nature Microbiology 2 (2017) No 16275.

[21] F. Liu, L. Csetenyi, G.M. Gadd, Amino acid secretion influences the size and composition of copper carbonate nanoparticles synthesized by ureolytic fungi, Applied Microbiology and Biotechnology 103 (2019) 7217-7230.

[22] Q. Li, D. Liu, Z. Jia, L. Csetenyi, Geoffrey M. Gadd, Fungal biomineralization of manganese as a novel source of electrochemical materials, Current Biology 26 (2016) 950-955.

[23] Q. Li, D. Liu, C. Chen, Z. Shao, H. Wang, J. Liu, Q. Zhang, G.M. Gadd, Experimental and geochemical simulation of nickel carbonate mineral precipitation by carbonate-laden ureolytic fungal culture supernatants, Environmental Science: Nano 6 (2019) 1866-1875.

[24] L. Krejčová, T. Leonhardt, F. Novotný, V. Bartůněk, V. Mazánek, D. Sedmidubský, Z. Sofer, M. Pumera, A metal-doped fungi-based biomaterial for advanced electrocatalysis, Chemistry – A European Journal 25 (2019) 3828-3834.

[25] Y. Hu, X. Peng, Z. Ai, F. Jia, L. Zhang, Liquid nitrogen activation of zero-valent iron and its enhanced Cr (VI) removal performance, Environmental Science & Technology 53 (2019) 8333-8341.

[26] A.K. Suresh, D.A. Pelletier, W. Wang, M.L. Broich, J.-W. Moon, B. Gu, D.P. Allison, D.C. Joy, T.J. Phelps, M.J. Doktycz, Biofabrication of discrete spherical gold nanoparticles using

the metal-reducing bacterium *Shewanella oneidensis*, *Acta Biomaterialia* 7 (2011) 2148-2152.

[27] B. Bajaj, B.D. Malhotra, S. Choi, Preparation and characterization of bio-functionalized iron oxide nanoparticles for biomedical application, *Thin Solid Films* 519 (2010) 1219-1223.

[28] J. Guo, R. Wang, W.W. Tjiu, J. Pan, T. Liu, Synthesis of Fe nanoparticles@graphene composites for environmental applications, *Journal of Hazardous Materials* 225-226 (2012) 63-73.

[29] C. Ding, W. Cheng, X. Nie, F. Yi, S. Xiang, A.M. Asiri, H.M. Marwani, Reactivity of carbonized fungi supported nanoscale zero-valent iron toward U(VI) influenced by naturally occurring ions, *Journal of Industrial and Engineering Chemistry* 61 (2018) 236-243.

[30] Y. Wang, H. Sun, X. Duan, H.M. Ang, M.O. Tadé, S. Wang, A new magnetic nano zero-valent iron encapsulated in carbon spheres for oxidative degradation of phenol, *Applied Catalysis B: Environmental* 172-173 (2015) 73-81.

[31] Y. Mu, F. Jia, Z. Ai, L. Zhang, Iron oxide shell mediated environmental remediation properties of nano zero-valent iron, *Environmental Science: Nano* 4 (2017) 27-45.

[32] H. Woo, J. Park, S. Lee, S. Lee, Effects of washing solution and drying condition on reactivity of nano-scale zero valent irons (nZVIs) synthesized by borohydride reduction, *Chemosphere* 97 (2014) 146-152.

[33] H.-S. Kim, T. Kim, J.-Y. Ahn, K.-Y. Hwang, J.-Y. Park, T.-T. Lim, I. Hwang, Aging characteristics and reactivity of two types of nanoscale zero-valent iron particles (Fe<sup>0</sup>BH and Fe<sup>0</sup>H<sub>2</sub>) in nitrate reduction, *Chemical Engineering Journal* 197 (2012) 16-23.

[34] Z. Zhu, Y. Xu, B. Qi, G. Zeng, P. Wu, G. Liu, W. Wang, F. Cui, Y. Sun, Adsorption-intensified degradation of organic pollutants over bifunctional  $\alpha$ -Fe@carbon nanofibres, *Environmental Science: Nano* 4 (2017) 302-306.

[35] P. Zhang, Y. Zhan, B. Cai, C. Hao, J. Wang, C. Liu, Z. Meng, Z. Yin, Q. Chen, Shape-controlled synthesis of Mn<sub>3</sub>O<sub>4</sub> nanocrystals and their catalysis of the degradation of methylene

blue, *Nano Research* 3 (2010) 235-243.

[36] H. Dong, Z. Cong, K. Hou, Y. Cheng, G. Zeng, Removal of trichloroethylene by biochar supported nanoscale zero-valent iron in aqueous solution, *Separation & Purification Technology* 188 (2017) 188-196.

[37] T. Phenrat, T. Thongboot, G.V. Lowry, Electromagnetic induction of zerovalent iron (ZVI) powder and nanoscale zerovalent iron (nZVI) particles enhances dechlorination of trichloroethylene in contaminated groundwater and soil: proof of concept, *Environmental Science & Technology* 50 (2015) 872-880.

[38] H. Tian, Y. Liang, T. Zhu, X. Zeng, Y. Sun, Surfactant-enhanced PEG-4000-NZVI for remediating trichloroethylene-contaminated soil, *Chemosphere* 195 (2018) 585-593.

[39] X. Zhao, W. Liu, Z. Cai, B. Han, T. Qian, D. Zhao, An overview of preparation and applications of stabilized zero-valent iron nanoparticles for soil and groundwater remediation, *Water Research* 100 (2016) 245-266.

[40] D.W. Green, B. Ben-Nissan, K.S. Yoon, B. Milthorpe, H.-S. Jung, Natural and synthetic coral biomineralization for human bone revitalization, *Trends in Biotechnology* 35 (2017) 43-54.

[41] L. Jie, C. Changlun, Z. Rui, W. Xiangke, Nanoscale zero-valent iron particles supported on reduced graphene oxides by using a plasma technique and their application for removal of heavy-metal ions, *Chemistry- An Asian Journal* 10 (2015) 1410-1417.

[42] W. Jiang, D.D. Dionysiou, M. Kong, Z. Liu, Q. Sui, S. Lyu, Utilization of formic acid in nanoscale zero valent iron-catalyzed Fenton system for carbon tetrachloride degradation, *Chemical Engineering Journal* 380 (2020) 122537-122544.

[43] X. Lv, H. Li, Y. Ma, H. Yang, Q. Yang, Degradation of carbon tetrachloride by nanoscale zero-valent iron@magnetic Fe<sub>3</sub>O<sub>4</sub>: impact of reaction condition, kinetics, thermodynamics and mechanism, *Applied Organometallic Chemistry* 32 (2018) e4139.

- [44] Y. Ma, X. Lv, Q.I. Yang, Y. Wang, X. Chen, Reduction of carbon tetrachloride by nanoscale palladized zero-valent iron@ graphene composites: kinetics, activation energy, effects of reaction conditions and degradation mechanism, *Applied Catalysis A: General* 542 (2017) 252-261.
- [45] X.-F. Wan, C. Guo, Y. Liu, X.-S. Chai, Y. Li, G. Chen, Kinetic research on dechlorinating dichlorobenzene in aqueous system by nano-scale nickel/iron loaded with CMC/NFC hydrogel, *Chemosphere* 194 (2018) 297-305.
- [46] L. Li, J. Hu, X. Shi, M. Fan, J. Luo, X. Wei, Nanoscale zero-valent metals: a review of synthesis, characterization, and applications to environmental remediation, *Environmental Science and Pollution Research* 23 (2016) 17880-17900.
- [47] Y. Ma, X. Lv, Q. Yang, Y. Wang, X. Chen, Reduction of carbon tetrachloride by nanoscale palladized zero-valent iron@graphene composites: kinetics, activation energy, effects of reaction conditions and degradation mechanism, *Applied Catalysis A: General* 542 (2017) 252-261.
- [48] Y. Zhou, L. Tang, G. Yang, G. Zeng, Y. Deng, B. Huang, Y. Cai, J. Tang, J. Wang, Y. Wu, Phosphorus-doped ordered mesoporous carbons embedded with Pd/Fe bimetal nanoparticles for the dechlorination of 2, 4-dichlorophenol, *Catalysis Science & Technology* 6 (2016) 1930-1939.